Study for the computational resolution of conservation equations of mass, momentum and energy

Application to solar receivers in Concentrated Solar Power plants

Giulio Beseghi
giulio.beseghi@tecnico.ulisboa.pt

Instituto Superior Técnico, Universidade de Lisboa, Portugal

November 2017

Abstract

The objective of the thesis is to provide a focused, comprehensive code based on Computational Fluid Dynamics to be applied to the study of natural and mixed convection of the air located outside an external cylindrical receiver of a Concentrating Solar Power (CSP) plant. CSP plants are a rapidly improving technology that is going to play an increasingly important role in electricity production in the decades to come. Convection of outer air in CSP plants represent a major concern mainly for two reasons: it must be solved to assess the thermal balance at the receiver and to calculate the local temperature of the materials; in fact, failure still represents an issue for the design of this component. The code will need to be able to describe both aspects. Therefore, a Direct Numerical Simulation approach is used, since it is able to solve thoroughly the three main equations that govern convection: the mass, momentum and energy conservation equations. In order to evaluate the change of the thermophysical properties due to the variation of temperature, a non-Boussinesq approach is proposed to solve the equations. After a contextualization of the external air convective losses of a Central Receiver System, the code is progressively built and validated, and a possible setup for its application to the thermal receiver is presented.
Keywords: Concentrating Solar Power; Computational Fluid Dynamics; Thermal receiver; Natural convection.

1. Introduction

Renewable electricity generation is rapidly growing, especially due to the push given by developing countries [1]. These technologies, as well as the traditional ones, require a deep understanding of the energy transfer processes in order to design the components to maximize the efficiency of the plant. A large majority of these transfer processes involve kinetic energy and heat transfer between fluids. Both processes depend on three equations that govern them: the mass, momentum, and energy conservation equations. In a vast majority of cases, an analytical solution of these equations cannot be found; therefore, two approaches can be used: the use of empirical correlations or the use of numerical simulation. Although the former are reliable since they come from physical evidence, they cannot provide a solution for a complex phenomenon that has a high-local dependence: turbulence is an example of chaotic, locally-dependent phenomenon that cannot be integrally modeled by the global approach of the correlations. In contrast, Computational Fluid Dynamics (CFD) can provide a local resolution of complex phenomena.

The aim of the thesis is the study of the natural convection (that is governed by the three equations mentioned) for the external air at a thermal receiver of a Concentrated Solar Power (CSP) plant. In the design of such plants, the prediction of locally-dependent variables as temperature and material stresses is crucial. Therefore, a CFD code able to compute (locally and globally) natural convection at a receiver will be developed. A Direct Numerical Simulation (DNS) will be used, given its reliability in the resolution of the governing equations. Moreover, convection will be solved with a model that considers the variation of air properties due to temperature, in contrast to the majority of the simulations available in the literature (according to Le Quéré et al. [14]).

2. Concentrated Solar Power – State of the Art & Economical Analysis

CSP is a technology that uses solar beam radiation to heat up a fluid that generates electricity

Table 1: Some characteristics of the main CSP configurations (state of the art) [22], [25].

	Parabolic trough	Solar tower	Linear Fresnel	Dish-Stirling
Maturity of Technology	Commercially proven	Commercially proven	Early commericial projects	Demonstration projects
Operating temperature [°C]	350-400	250-565	250-350	550-750
Global efficiency [η]	0.1-0.16	0.1-0.22	0.8-0.12	0.16-0.29
Receiver/absorber	Moving with collector	Fixed	Fixed	Moving with collector
Outlook for improvements	Limited	Very Significant	significant	High (through mass production)
Advantages	Mature technology, Modular units	High η, Compatible with Brayton cycle	Fixed, Low investment costs	High η, Modular units, Compatible with Brayton cycle
Disadvantages	Relatively low η	High O&M costs	Relatively low η	No thermal storage available, low maturity

by undergoing a thermodynamic cycle. There are four main configurations of CSP plants: Parabolic Trough Collector (PTC), Linear Fresnel Reflector (LFR), Central Receiver System (CRS) and Parabolic Dish System (PDS). Two main components of a CSP plant are the **collector** and the **receiver**: the former is responsible for collecting the sun radiation, and the latter for its absorption. The solar energy absorbed is then transfered to a Heat-Transfer Fluid (HTF). PTC is the most mature technology: it consists in a set of one-axis tracking parabolic mirrors that focus the sun rays onto the selective surface of the receiver tube. The receiver moves in tandem with the collector. LFRs are similar, but use flat mirrors recreating a parabola as collectors; differently from PTCs, the receiver is fixed. CRSs use a field of flat two-axes tracking mirrors (called heliostats) to focus solar radiation onto a single central receiver located at the top of a tower. PDSs consist in two-axes tracking paraboloid-shaped mirrors that focus solar radiation onto a Stirling engine.

Both collector and receiver require a high level of technology. Regarding collectors, R&D is trying to improve materials reflectivity to develop efficient mirrors; moreover, it is struggling to reduce the investment cost: on the one side by reducing the manufacture process complexity, on the other side by estimating the optimal size of the mirrors. The development of efficacious dust-cleaning technologies could help to maintain a high efficiency throughout the operative life of the plant. PTC receivers' main objective is to guarantee a high rate of absorption of solar radiation and simultaneously a low rate of emission. This is accomplished with solar-transparent glass enclosing a selective surface, being the two separated by a vacuum (or air) zone. CRS's receivers are divided into tubular and volumetric receivers. The former are composed of a set of tubes in which the HTF flows and absorbs the incoming energy. The latter use a porous medium that absorbs solar radiation and passes it to external air sucked from ambient. Tubular receivers divide in external and cavity receiver; the difference is that the former is put in direct contact with the atmosphere, while the second is enclosed by a cavity. Volumetric receivers divide in open vol-

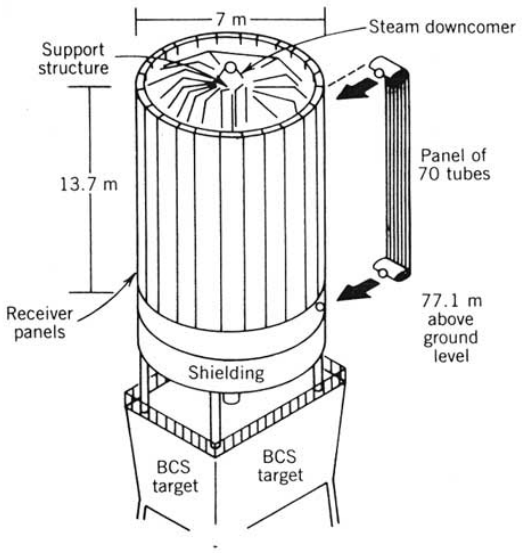

Figure 1: Example of an external cylindrical receiver

umetric and closed (or pressurized) volumetric receivers. The former suck air at ambient pressure; therefore, heated air has to exchange energy in a heat exchanger with a second fluid undergoing the thermodynamic cycle. The latter instead, drive air mechanically into the receiver, pressurizing it; heated air can be used directly in a Brayton cycle.

The most used HTFs are air, steam and molten salt; the selection of the fluid must consider costs and thermodynamic properties: low viscosity, high conductivity and low thermal degradation are generally sought. HTFs should also be characterized by a good heat removal capability, that is crucial when Thermal Energy Storage (TES) is present. TES consists in storing the energy absorbed by the heated fluid to extend the operation of the plant and increase its output: in fact, solar radiation is available only for a number of hours every day. It is

said to be direct if the fluid used to store energy is the one used to collect it, and indirect otherwise. Energy can be stored as sensible heat, latent heat or thermo-chemical heat. The former is based on internal energy variation due to temperature differences while the second due to phase change; the third, instead, is based on a thermo-chemical reaction. The Single-Tank Thermocline System is a particular type of storage that exploits the buoyancy effects of the HTF to store energy in a solid medium. TES is particularly interesting for CRSs, since temperatures in these plants are higher, giving the possibility to store more energy per tank.

The use of renewable technologies is rapidly growing for two reasons: on the one hand, governments are pushing clean technologies concerned for climate issues; on the other hand, the technologies per se are becoming more and more profitable. CSP is expected to boost its installed power by 2040, when it is expected to produce about 200 times the energy it produces nowadays, especially due to the progress of the CRS configuration [13]. CSP is particularly present in two countries: Spain and United States. This is the result of three processes: the effort in R&D that both countries put, the economic incentives given by the governments and an important amount solar resource, measured as the Direct Normal Irradiance (DNI). DNI is a parameter that measures the average direct solar energy that hits a specific location. "Direct" refers to the share of solar radiation that has not interacted with the atmosphere and maintained its original direction; this radiation is the one that can be focused on a CSP receiver. Many developing countries have a high DNI, making CSP an even more interesting technology: if the cost reduction trend keeps on occurring, such countries could adopt this technology; this is already happening (for example, in China and Chile, where several projects have been commissioned) [12]. One of the main issues of CSP is that it is put in direct competition with PV energy, since both rely on solar energy. PV has been undergoing a rapid cost reduction that is expected to continue. To compete with this technology (and the traditional ones), it is crucial for CSP to improve TES systems: in fact, on the one hand, TES improves the dispatchability and reliability of the renewable technology (something that cannot be achieved by PV without the use of batteries, still too expensive); on the other hand, makes it possible to maintain the electricity production in the afternoon, when the electricity offer is lower and sales more profitable. Since CRSs are currently expected to be the most successful CSP technology [13], they will be investigated in this thesis.

3. Concentrated Solar Power – Optical and Thermal losses

Before the development of the code regarding natural convection, the plant losses at the collector and receiver are explained. This can help to contextualize the role of convection among all the heat losses that happen outside the plant. The first loss that occurs to solar radiation takes place when it enters Earth's atmosphere. The phenomenon is known as scattering: a certain amount of radiation is deviated by the atmosphere particles and loses its original direction. This deviated radiation cannot be used in a CSP plant because it cannot be pointed to the receiver; the remaining part, which is the one that the plant can exploit, is called beam (or direct) radiation. Beam radiation is reflected towards the receiver; however, a significant part of it is lost in the path. All the losses that occur in the path from the collector to the receiver are called **optical losses**. Firstly, the cosine losses express the part of the radiation that is lost due to the fact that mirrors are not perpendicular to sun rays, so their effective area is lower. An efficiency can be associated with the process: $\eta_{cos} = \cos\theta$, where θ is the angle between the direction of the rays and the normal to the surface of the heliostats. Then, the reflectivity losses express the energy lost due to the absorption of the heliostats: the efficiency associated is $\eta_{ref} = \rho_h$, where ρ_h is the reflectivity of the heliostats. Part of energy reflected by a heliostat can be blocked by others placed near; moreover, some mirrors can put others partially in shade. The efficiency related to the blocking/shading phenomenon is $\eta_{bs} = 1 - \frac{\text{blocked and shaded surface}}{\text{total surface}}$. Part of the solar radiation reflected by the heliostats is absorbed by the atmosphere (the phenomenon is called atmospheric attenuation). According to the Pitman and Vant-Hull model [3], the efficiency associated is $\eta_{atm} = \tau_{atm} = e^{-\xi\, R^S}$, where τ_{atm} is the air transmittance, R is the slant range, ξ is the the broadband extinction coefficient, and S is a proportionality constant. Finally, the spillage losses are caused by the non-perfect pointing of the radiation to the receiver [18]. Their associated efficiency is $\eta_{spil} = \frac{1}{2\pi\cdot\sigma_{tot}^2} \int_x \int_y e^{-\frac{x^2+y^2}{2\,\sigma_{tot}^2}}\, dy\, dx$, where σ_{tot} represents the standard deviation that characterizes the radiation dispersion. Combining all the losses, the optical losses become

$$\eta_{opt} = \eta_{cos}\, \eta_{ref}\, \eta_{bs}\, \eta_{atm}\, \eta_{spil} \tag{1}$$

Before being absorbed by the HTF, the energy incident on the receiver undergoes other losses, that are called **thermal losses**. The absorption losses are given by the partial reflection of this amount of energy at the receiver: $\dot{Q}_{ref} = \rho_r \dot{Q}_{in}$, where ρ_r

is the reflectivity of the receiver. Then, the convective losses are due to the energy that is transfered to the air surrounding the receiver: $\dot{Q}_{conv} = h\,(T_r - T_{amb})\,A_r$, where h is the heat transfer coefficient between the receiver and air, T_r is the receiver temperature, T_{amb} is ambient temperature and A_r is the receiver surface. h is evaluated with the correlation given by Siebers & Kraabal [19] that takes into account forced and natural convection. For cylindrical receivers, the heat transfer coefficient can be expressed as a function of the values it would take if forced convection ($\bar{h}_f$) and natural convection ($\bar{h}_n$) were considered separately: $\bar{h} = \left(\bar{h}_f^{3.2} + \bar{h}_n^{3.2}\right)^{1/3.2}$. Forced convection is calculated with a correlation of a cross-flow on a cylinder with pyramidal shaped roughness elements, that expresses $\overline{h}_f$ as a function of the Reynolds $Re_D = \frac{\rho\,u\,D}{\mu}$ and Nusselt number $Nu_D = \frac{h_f\,D}{k}$ relative to the diameter D of the receiver. Natural convection is calculated with a correlation for a vertical flat plate, that expresses $\overline{h}_n$ as a function of the Grashof $Gr_H = \frac{\rho^2\,g\,\beta\,(T_r - T_{amb})\,H^3}{\mu^2}$ and Nusselt number $Nu_H = \frac{h_n\,H}{k}$ relative to the height H of the receiver. Finally, part of the energy captured by the receiver is lost as thermal radiation. Assuming the ambient a black body and the receiver a diffuse surface, the radiative losses can be expressed as $\dot{Q}_{rad} = \varepsilon_r\,\sigma\,\left(T_r^4 - T_{sg}^4\right)\,A_r$, where ε_r is the emissivity of the receiver, σ is the Boltzmann constant and T_{sg} is the average sky-ground temperature. A global thermal efficiency can be defined as

$$\eta_{th} = \frac{\dot{Q}_{in} - \dot{Q}_{ref} - \dot{Q}_{cond} - \dot{Q}_{conv} - \dot{Q}_{rad}}{\dot{Q}_{in}} \qquad (2)$$

Acknowledged these losses, a simulation is performed on an illustrative plant (having an external cylindrical receiver). The characteristics of the plant are mainly extracted from a paper describing the *Solar Two* CRS plant [17]; the ones not reported are assumed consulting the literature. The results are reported in tab. 2. Then, a sensitivity analysis that recreates the different conditions at which the plant can operate is performed. The cosine losses are demonstrated to have a great influence, suggesting that during the plant design the optimization of the heliostat disposition is a major concern; moreover, it is shown that there is always a temperature of the receiver that optimizes the global efficiency of the plant; furthermore, both the receiver absorptance and emissivity show to play an important role in the optimization of the plant efficiency. Convection is demonstrated to play an important role among the thermal losses, as shown in tab. 2 (it counts for around the 10%). Moreover, convection losses can become the most impacting thermal loss when the wind velocity is major than a certain value.

Table 2: Base case results – efficiency and heat balance.

	Efficiency [%]		Heat [MW]
η_{cos}	86.6	$\dot{Q}_{sol}$	61.05
η_{ref}	90.8	$\dot{Q}_{in}$	44.18
η_{bs}	93.0	$\dot{Q}_{r,\,ref}$	0.52
η_{atm}	99.3	$\dot{Q}_{conv}$	0.20
η_{spil}	99.0	$\dot{Q}_{rad}$	1.67
η_{opt}	72.4	$\dot{Q}_u$	41.79
η_{th}	94.6		
$\eta_{overall}$	68.5		

The procedure followed considered natural convection as a global process, through the use of a general correlation. However, convection at a thermal receiver always involves a high rate of turbulence, that cannot be fully described with a global approach. Turbulence causes a spacial-dependent distribution of temperature and fluid velocity, that can lead to local overheating and, eventually, failure of the receiver. Therefore, it is clear that convection must be solved with a more powerful tool, that can describe it both locally and globally.

Therefore, a CFD code to describe natural convection at a receiver of a CRS is proposed. As explained in the introduction, it consists in a DNS that considers the dependence of the air thermophysical properties on the temperature; this approach particularly suitable for the study of natural convection of a receiver, where temperature gradients are usually very high.

4. Mathematical Formulation

The main equations that govern the flow of a fluid and its energy transfer processes are three: the mass, momentum and energy conservation equations. All can be viewed as a particular case of a single equation: the **convection-diffusion equation**

$$\frac{\partial(\rho\,\phi)}{\partial t} + \nabla\cdot(\rho\,\mathbf{u}\,\phi) = \nabla\cdot(\Gamma\,\nabla\phi) + S_\phi \qquad (3)$$

where ρ is the fluid density, ϕ is the variable of interest, $\mathbf{u}$ is the velocity vector, Γ is the diffusion coefficient and S_ϕ is the source term. The mass, momentum, and energy equations are presented for incompressible fluids: in fact, in convection problems the effects of the compressibility of the air can be neglected. For such fluids, the mass equation is

$$\nabla\cdot\mathbf{u} = 0 \qquad (4)$$

The momentum equation (also known as the Navier-Stokes equation for incompressible fluids) can be expressed as the function of the rate-of-

strain tensor $\mathbf{S} = \frac{1}{2}\left(\nabla\mathbf{u} + \nabla\mathbf{u}^{\mathrm{T}}\right)$:

$$\rho\,\frac{\partial \mathbf{u}}{\partial t} + \rho\,(\mathbf{u}\cdot\nabla)\,\mathbf{u} = -\nabla p + \nabla\cdot(2\,\mu\,\mathbf{S}) + \rho\,\mathbf{g} \quad (5)$$

where $\mathbf{g}$ is the gravity acceleration, p is the pressure and μ the viscosity of the fluid. In case the viscosity is constant, the equation becomes

$$\rho\,\frac{\partial \mathbf{u}}{\partial t} + \rho\,(\mathbf{u}\cdot\nabla)\,\mathbf{u} = -\nabla p + \mu\,\nabla^2\mathbf{u} + \rho\,\mathbf{g} \quad (6)$$

The energy equation can be expressed as

$$\rho\,c_P\,\frac{\partial T}{\partial t} + \rho\,c_P\,\mathbf{u}\cdot\nabla T = \nabla\cdot(k\,\nabla T) - \nabla\cdot\dot{\mathbf{q}}^R \quad (7)$$

where c_P is the specific heat, T is the temperature, k is the conductivity and $\nabla\cdot\dot{\mathbf{q}}^R$ represents the sum of the incoming heat without considering conduction. The Boussinesq approximation is a simplification of the momentum and energy equations, that states that the thermophysical properties can be considered constant except density in the buoyancy forces (the term $\rho\,\mathbf{g}$). In the buoyancy forces, the density can be assumed linear with the temperature $\rho_0\,[1-\beta\,(T-T_0)]\,\mathbf{g}$; this simplifies the momentum and the energy equations to

$$\rho_0\,\frac{\partial \mathbf{u}}{\partial t} + \rho_0\,(\mathbf{u}\cdot\nabla)\,\mathbf{u} = -\nabla p' + \mu\,\nabla^2\mathbf{u} - \rho_0\,\beta\,(T-T_0)\,\mathbf{g} \quad (8)$$

$$\rho_0\,c_P\,\frac{\partial T}{\partial t} + \rho_0\,c_P\,\mathbf{u}\cdot\nabla T = k\,\nabla^2 T - \nabla\cdot\dot{\mathbf{q}}^R \quad (9)$$

The Boussinesq approximation simplifies significantly the computation, and it is generally assumed to be valid for a low temperature range $\Delta T_{max} = 10\,K$. The last equation analyzed (still a convection-diffusion equation) describes conduction in solids:

$$\rho\,c_P\,\frac{\partial T}{\partial t} = \nabla\cdot(k\,\nabla T) - \nabla\cdot\dot{\mathbf{q}}^R \quad (10)$$

It is important to model conduction in thermal receivers because it governs the heat transfer between hotter and colder sections of the receiver (so it must be taken into account to compute the temperature distribution at the receiver panels).

5. Numerical Methodology

The discretization method used in the codes is the Finite Volume Method (FVM). This method is particularly effective when used to solve simple geometries. The domain is divided in a certain number of control volumes. For every volume, a unique thermodynamic state is defined. The volumes are connected with a grid; the nodes of the grid represent a single control volume and are located at their center: for this reason, the approach is called *node centered*. The grid is said to be *structured*, since it is characterized by a regular connectivity. In FVM, properties are evaluated at the center of the volume, whereas flows are evaluated at the surfaces of the volume.

Both explicit and implicit time-discretization methods are presented: in the former, the unknowns are expressed as a function of known variables; in the latter, at least one unknown is a function of other unknowns. A disadvantage of explicit methods is that the time step selected cannot exceed a certain value, defined by the Courant-Friedrichs-Lewy (CFL) conditions [6]. The value is usually really small, hence it increases dramatically the computational time of the code. In this work, implicit problems are solved with a line-by-line Tri-Diagonal Matrix Algorithm (TDMA). In case the third dimension is considered, the line-by-line algorithm is looped with a Gauss-Siedel algorithm. Both TDMA and algorithms are described by Conte & Boor [5].

In parallel to the mesh presented, another type of mesh is used. In fact, all the velocity components are defined at the walls of the control volumes of the main mesh (as shown in fig. 2). The

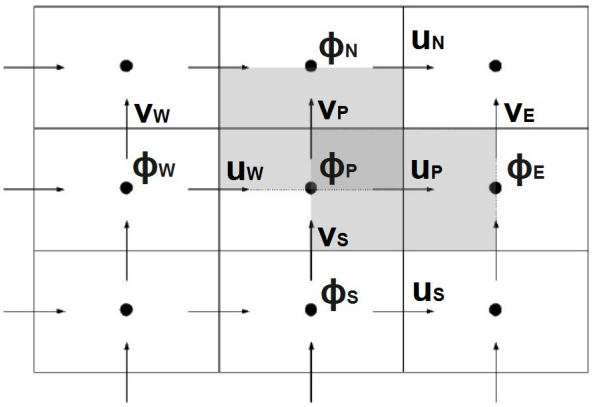

Figure 2: Staggered mesh. The gray areas represent the x and y staggered control volumes.

shifted mesh created is called *staggered mesh*. In contrast, the main mesh is called *collocated mesh*. Except the velocities (and consequently the mass flows), all the properties are defined in correspondence to the collocated mesh.

6. Heat Transfer Processes – Computational Study

The code for the analysis of natural convection is built from scratch. To validate it, it is necessary to solve some benchmark problems and verify that the results obtained are close to the solution given by other authors.

The first two problems regard the convection-diffusion equation. The first is a problem of 2D conduction (a type of heat diffusion, occurring in solids). The goal is to solve the unsteady heat transfer at a rod composed of four materials having

different thermophysical properties. The problem

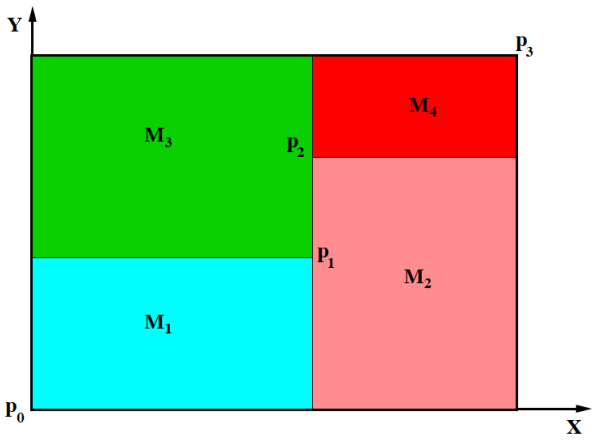

Figure 3: Section of the rod, showing the four materials it is composed of.

is solved with a constant, collocated mesh. Three time-discretization methods are investigated: the explicit Euler, the implicit Euler and the Crank-Nicolson method. The first two methods are first-order, while the second is second-order. The results obtained with the three methods are compared with the reference solution. Since the differences are really small, the three of them are considered to be correct.

The second problem regards the resolution of the convection-diffusion equation for a given flow. It is known as the Smith-Hutton problem [21]. The flow is shown in fig. 4. The problem introduces

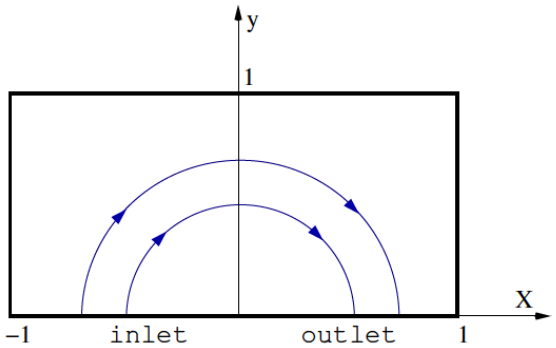

Figure 4: Smith-Hutton problem configuration. Figure retrieved from Smith & Hutton [21].

the need for a convection scheme to evaluate the mass flow at the surfaces of the control volumes. In fact, with this configuration the staggered mesh is not used: the velocity components are referred to a regular collocated mesh. The velocity value at the surfaces is obtained by interpolation performed with a convective scheme. Five convective schemes are presented: the Upwind Difference Scheme (UDS), the Central Difference Scheme (CDS), the Second-order Upwind Difference Scheme (SUDS), the Quadratic Upstream Interpolation for Convective Kinematics scheme (QUICK), and the Sharp and Monotonic Algorithm for Realistic Transport (SMART). The results are compared with a benchmark solution. The SMART scheme demonstrates to be the most precise one; moreover, it is the only scheme that does not present unrealistic energy damping or evident unphysical distributions of the unknown property ϕ. Therefore, it is selected to be the convective scheme applied to the next convective problems.

The next two problems analyzed introduce the computation of laminar flows. The first one is the 2D driven cavity problem. The benchmark solution is given by Ghia, Ghia & Shin [11]. The goal is to solve the fluid flow in a cavity whose upper wall is moving at a constant velocity. The problem

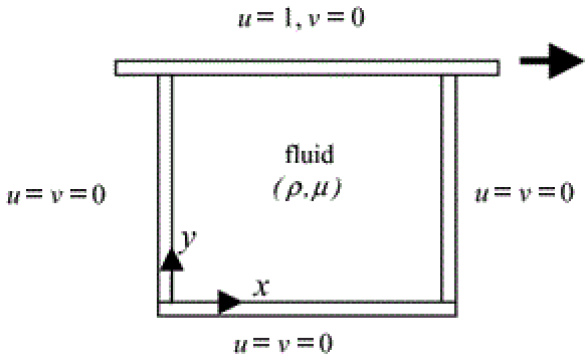

Figure 5: Horizontal section of the driven cavity. Figure retrieved from Marchi, Suero & Araki [15].

is solved with the Fractional Step Method (FSM), firstly introduced by Chorin [4], in which the momentum equation is projected on a free-divergence space. The velocity and pressure fields are computed in the following way:

1. a projection velocity $\mathbf{u}^p$ is introduced and computed with a second-order backward Adams-Bashorth method;
2. the pressure field, expressed as a function of the projection velocity, is computed implicitly solving a Poisson equation;
3. the velocity field is computed (as a function of the pressure and projection velocity), applying the projection velocity definition.

The solution of the problem depends on the Reynolds number: results for Reynolds ranging from 100 to 7500 are presented. The velocity variation at the mid horizontal and vertical axes is compared to the benchmark solution: no relevant differences are found, and the code is validated.

The energy conservation equation is introduced with the Differentially Heated Cavity (DHC) problem. At first, the Boussinesq approximation is assumed. The goal is to solve natural convection of air inside a cavity having two isothermal

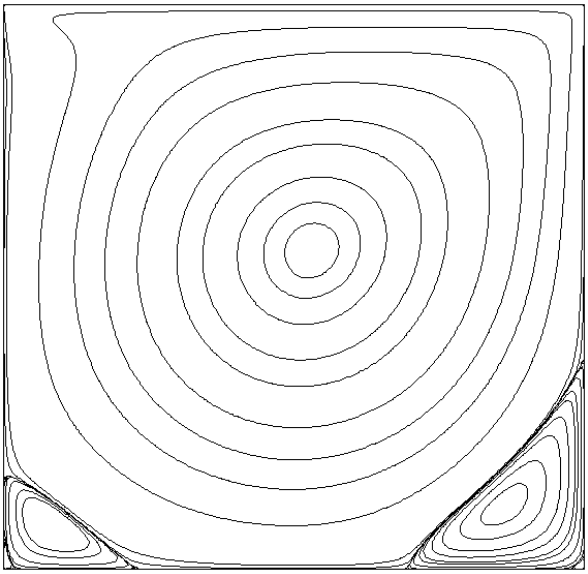

Figure 6: Laminar driven cavity problem – stream function ψ map ($Re = 1000$, mesh 256×256)

vertical walls and two adiabatic horizontal walls. The nature of the problem depends on the non-dimensional number Rayleigh defined as $Ra = Gr\,Pr$. The Grashof number Gr has been already presented in sec. 3. The Prandtl number is defined as $Pr = \frac{mu\,c_P}{k}$. The energy equation (eq. 7)

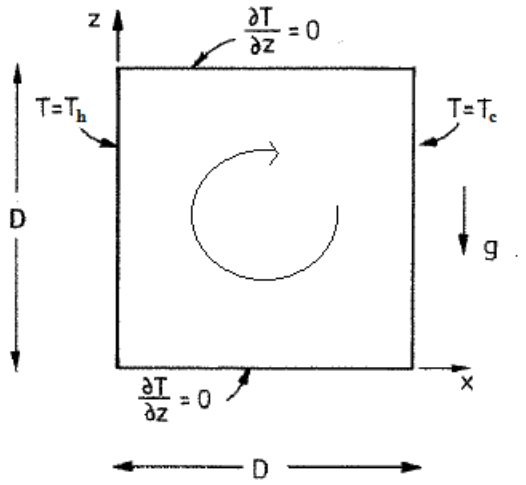

Figure 7: Differentially Heated Cavity, section of the vertical plane. Figure edited from de Vahl Davis & Jones [8].

is solved with a second-order backward Adams-Bashforth method. Then, FSM is applied to the momentum and continuity equation. The stream function, velocity components, and Nusselt number at significant locations are compared with the reference solution given by De Vahl Davis [8], [7]. The results agree with the benchmark solution, meaning that the code is validated. Then, the Boussinesq approximation is abandoned; in fact, the approach is considered to be valid only for a limited range of temperature. The approximation would not obviously verify in the study of the thermal receiver of a CRS plant: in fact, the temperature difference between the receiver and ambient air usually exceeds $300\,K$ (compare tab. 1). Therefore, a different approach is used: the thermophysical properties are assumed to depend on the temperature following the correlations given by Eckert & Drake [9]. The study is repeated, considering the same temperature range. The results obtained are almost identical to the previous ones, so the model is assumed to be correct. Finally, the study is extended to a 3D case. The marked increase in the number of nodes makes the computational time grow significantly: in order to keep it low, a non-constant mesh is defined. In this mesh, node spacing follows a hyperbolic function distribution, depending on the concentration factor γ:

$$x_w[i] = \frac{D}{2}\left\{1 + \frac{\tanh\left[\gamma\left(2\,\frac{i-1}{N} - 1\right)\right]}{\tanh\gamma}\right\} \quad (11)$$

where $x_w[i]$ represents the west face x-coordinate of the control volume associated to the i-th horizontal node. This mesh has the advantage that resolves appropriately the flow at the wall. That region has to be well-resolved because it is characterized by steep gradients of temperature and velocity (a boundary layer is created). The results obtained are compared with the 2D case, concluding that the 3D computation is correct.

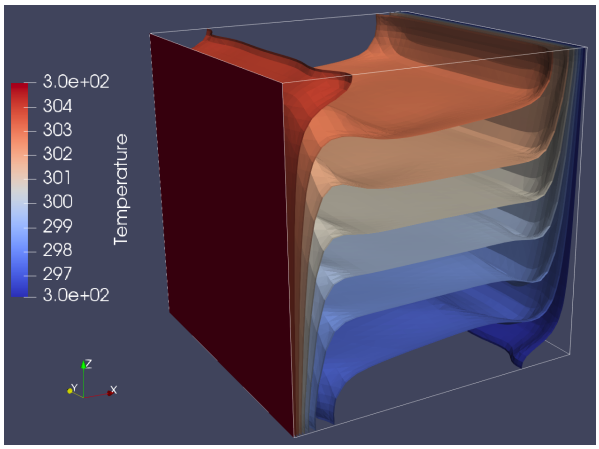

Figure 8: 3D DHC temperature map (variable thermophysical properties), isothermal surfaces for $Ra = 10^6$.

Finally, turbulence is introduced in the driven cavity and the Differentially Heated Cavity problems. The mesh is defined to solve appropriately the thin boundary layers that form at the walls characterized by high gradients of velocity (and temperature); to do so, the method described by Zhang et al. [26] is used: the viscous sublayer (which is

the zone of the boundary layer that is put in direct contact with the wall) is discretized with a sufficient number of nodes. The method is based on the computation of the wall shear stresses, since the latter influence the viscous sublayer thickness.

In the driven cavity problem, turbulence arises when $Re \approx 8000$. The flow at the cavity becomes unsteady: in particular, the eddies created at the corners of the cavity become unstable, and they start to separate periodically. This leads to a periodic global flow: the whole velocity field oscillates at a particular frequency. Averaged solutions and frequency of oscillation are compared to benchmark solutions [10], [2]: the results are very similar, and the conclusion is that the code developed also works in turbulent flow problems. To have

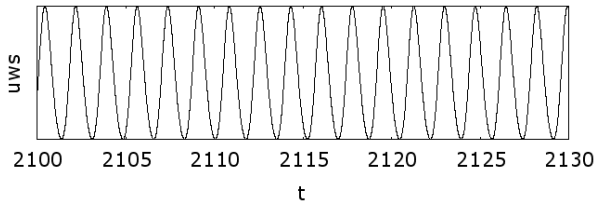

Figure 9: Time oscillation of the horizontal component of the velocity at a specific location of the cavity.

a further confirmation, the turbulent Differentially Heated Cavity problem is analyzed. Turbulence arises when $Ra \approx 1.03 \cdot 10^8$. Both the 2D and 3D codes that consider the effect of the variable thermophysical properties are verified with a benchmark case; however, the 3D problem shows some minor discrepancies from the reference due to a different definition of the boundary conditions.

The DNS codes are ready to be modified to be applied to a case of natural convection occurring at the receiver of a CSP plant. However, an approach different from the DNS is analyzed: the Large Eddy Simulation approach. This method is considered because, even though it is not as precise as DNS, it can reduce significantly the computational costs if well-implemented. The LES approach to turbulence consists in the modelization of the smallest scales of motion: energy dissipation at small scales is artificially carried out by filtering the momentum conservation equation. Five well-known LES models are implemented: the Smagorinsky model [20], the WALE model [16], the Vreman's model [24] and the Verstappen's model [23]. However, the code computation crashes for the models different than the Smagorinsky model. Moreover, the latter demonstrates to be unsuitable to solve problems that have a high dependence on the boundary conditions. A correction of the part of the code relative to the other four LES models is left as a possible future improvement.

7. Setup for the Application of the Codes to a Thermal Receiver

Having verified the DNS code developed, a possible application for the study of an external cylindrical receiver is presented. The computation is not performed because the resources available make it impossible to provide a solution of the problem; in fact, the elevated degree of turbulence requires a suitable mesh that should consist in a too elevated number of nodes to compute a result in a reasonable amount of time. However, a 2D approach is presented below. The region affected by natural

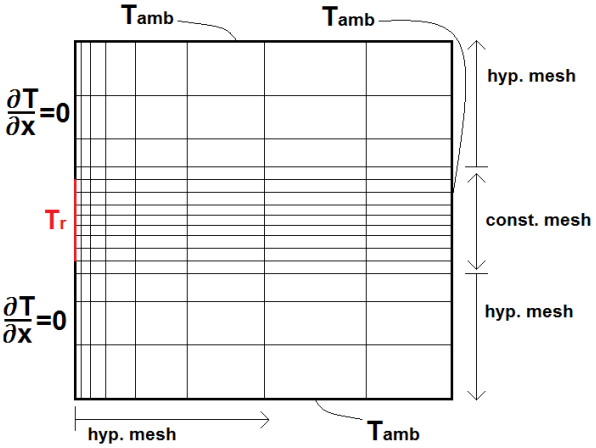

Figure 10: Mesh and boundary conditions definition for the computational study of natural convection in a cylindrical tubular receiver. The red line corresponds to a simplified panel of the receiver.

convection can be assumed to be a cavity. In this model, the vertical west wall tries to recreate a flat panel of the tubular receiver. The central section corresponds to the receiver itself, having the average temperature of $\overline{T}_r$; the upper and lower sections of the wall correspond to fictitious adiabatic walls. The three other walls represent three fictitious walls having a temperature equal to T_{amb}. The role of the fictitious walls is to recreate the phenomena occurring in the real convection at the receiver: the adiabatic walls drive the hot flux upwards, without introducing nor dissipating energy; the walls at ambient temperature "artificially damp" the energy absorbed by air, recreating the dispersion of the hot fluid in the ambient. It is *crucial* that the fictitious walls have no noticeable effect on the flow close to the receiver panel, where a potential Nusselt study can be performed. For this reason, the energy-damping walls have to be put sufficiently distant from the receiver: their placement at a farther position should not change the convective losses at the receiver. The boundary layer at the hot panel must be well-resolved; an adjusted version of the hyperbolic mesh described by eq. 11 can be used. The same mesh function can be used to design the vertical spacing for y coordinates be-

tween the receiver and the horizontal walls; vertical spacing at the receiver can be constant, as shown in fig. 10.

8. Conclusion

Although it has not been possible to apply the code developed directly to a thermal receiver, the code has been demonstrated to work properly being put in comparison with relevant benchmark cases; then, a possible presentation of the application to natural convection has been presented. The computational structure developed represents an efficient tool, tailored in order to be able to be applied to solve natural convection problems that arise in a thermal receiver of a CSP plant. The code gives a strong result since it can provide the instant (or time-averaged) values of:

- the local and global values of the heat transfer (through the Nusselt number);
- the velocity, temperature and pressure field throughout the whole domain;
- the local viscosity, conductivity and density of the fluid;
- the shear stress at the walls τ_w.

The computation of the fields is particularly precise, since it is carried out through a DNS, that fully solves the three equations.

The code developed still presents many limitations, that must be acknowledged for a future use. Its biggest limitation was the impossibility of testing it with a real case of convection: this operation is needed to confirm that the assumptions made are correct. Moreover, in the discussion of the setup for the application of the code to the receiver the temperature of the receiver $\overline{T}_r$ was assumed to be constant. The real distribution of temperature could be computed by solving the thermal balance at the receiver: to do so, the code developed could be modified to supply a version able to be applied to the forced convection of the HTF flowing in the tubes of the receiver. The code presented could also be modified to solve forced convection cases; in that case, a 3D simulation would become compulsory. Moreover, a more suitable mesh should be defined. Parallelization of the code should be considered, in order to dramatically reduce the computational time. Finally, the LES code could be corrected, giving the possibility to use it as an alternative to the DNS.

References

[1] OECD (2017), renewable energy (indicator). Accessed on 10 August 2017.

[2] C.-H. Bruneau and M. Saad. The 2d lid-driven cavity problem revisited. *Computers & Fluids*, 35(3):326–348, 2006. Accessed on 3 October 2017.

[3] J. Cardemil, A. Starke, V. Scariot, I. Grams, and S. Colle. Evaluating solar radiation attenuation models to assess the effects of climate and geographical location on the heliostat field efficiency in brazil. *Energy Procedia*, 49:1288–1297, 2014. Proceedings of the SolarPACES 2013 International Conference, Accessed on 5 September 2017.

[4] A. J. Chorin. Numerical solution of the navier-stokes equations. *Mathematics of computation*, 22(104):745–762, 1968. Accessed on 21 September 2017.

[5] S. D. Conte and C. W. D. Boor. *Elementary Numerical Analysis: An Algorithmic Approach*. McGraw-Hill Higher Education, 3rd edition, 1980. Accessed on 16 September 2017.

[6] R. Courant, K. Friedrichs, and H. Lewy. On the partial difference equations of mathematical physics. *IBM journal of Research and Development*, 11(2):215–234, 1967. Accessed on 13 September 2017.

[7] G. de Vahl Davis. Natural convection of air in a square cavity: a bench mark numerical solution. *International Journal for numerical methods in fluids*, 3(3):249–264, 1983. Accessed on 24 September 2017.

[8] G. de Vahl Davis and I. Jones. Natural convection in a square cavity: a comparison exercise. *International Journal for numerical methods in fluids*, 3(3):227–248, 1983. Accessed on 24 September 2017.

[9] E. R. G. Eckert and R. M. Drake Jr. *Analysis of heat and mass transfer*. Hemisphere Publishing, 1987. Accessed on 6 September 2017.

[10] E. Erturk, T. C. Corke, and C. Gökçöl. Numerical solutions of 2-d steady incompressible driven cavity flow at high reynolds numbers. *International Journal for Numerical Methods in Fluids*, 48(7):747–774, 2005. Accessed on 3 October 2017.

[11] U. Ghia, K. N. Ghia, and C. Shin. High-re solutions for incompressible flow using the navier-stokes equations and a multigrid method. *Journal of computational physics*, 48(3):387–411, 1982. Accessed on 19 September 2017.

[12] HELIOSCSP. Database of concentrated solar power projects all around the world. Accessed 25 October 2017.

[13] International Energy Agency. World energy outlook. 2015. Accessed on 22 August 2017.

[14] P. Le Quéré, C. Weisman, H. Paillère, J. Vierendeels, E. Dick, R. Becker, M. Braack, and J. Locke. Modelling of natural convection flows with large temperature differences: A benchmark problem for low mach number solvers. part 1. reference solutions. *ESAIM: Mathematical Modelling and Numerical Analysis*, 39(3):609–616, 2005. Accessed on 27 October 2017.

[15] C. H. Marchi, R. Suero, and L. K. Araki. The lid-driven square cavity flow: numerical solution with a 1024 x 1024 grid. *Journal of the Brazilian Society of Mechanical Sciences and Engineering*, 31(3):186–198, 2009. Accessed 25 October 2017.

[16] F. Nicoud and F. Ducros. Subgrid-scale stress modelling based on the square of the velocity gradient tensor. *Flow, Turbulence and Combustion*, 62(3):183–200, 1999. Accessed on 18 October 2017.

[17] J. E. Pacheco, R. Bradshaw, D. Dawson, W. De la Rosa, R. Gilbert, S. Goods, M. Hale, P. Jacobs, S. A. Jones, G. J. Kolb, et al. Final test and evaluation results from the solar two project. *Report No. SAND2002-0120, Sandia National Laboratories*, 45, 2002. Accessed on 6 September 2017.

[18] M. Schmitz, P. Schwarzbözl, R. Buck, and R. Pitz-Paal. Assessment of the potential improvement due to multiple apertures in central receiver systems with secondary concentrators. *Solar Energy*, 80(1):111–120, 2006. Accessed on 5 September 2017.

[19] D. L. Siebers and J. S. Kraabel. Estimating convective energy losses from solar central receivers. Technical report, Sandia National Labs., Livermore, CA (USA), 1984. Accessed on 5 September 2017.

[20] J. Smagorinsky. General circulation experiments with the primitive equations: I. the basic experiment. *Monthly weather review*, 91(3):99–164, 1963. Accessed on 18 October 2017.

[21] R. Smith and A. Hutton. The numerical treatment of advection: A performance comparison of current methods. *Numerical Heat Transfer, Part A Applications*, 5(4):439–461, 1982. Accessed on 16 September 2017.

[22] M. Taylor, K. Daniel, A. Ilas, and E. Y. So. Renewable power generation costs in 2014. *International Renewable Energy Agency*, 2015. Accessed on 27 October 2017.

[23] R. Verstappen. When does eddy viscosity damp subfilter scales sufficiently? *Journal of Scientific Computing*, 49(1):94, 2011. Accessed on 18 October 2017.

[24] A. W. Vreman. An eddy-viscosity subgrid-scale model for turbulent shear flow: Algebraic theory and applications. *Physics of Fluids*, 16(10):3670–3681, 2004. Accessed on 18 October 2017.

[25] X. Xu, K. Vignarooban, B. Xu, K. Hsu, and A. M. Kannan. Prospects and problems of concentrating solar power technologies for power generation in the desert regions. *Renewable and Sustainable Energy Reviews*, 53:1106–1131, 2016. Accessed on 15 August 2017.

[26] H. Zhang, F. X. Trias, A. Gorobets, Y. Tan, and A. Oliva. Direct numerical simulation of a fully developed turbulent square duct flow up to re$_\tau$= 1200. *International Journal of Heat and Fluid Flow*, 54:258–267, 2015. Accessed on 8 October 2017.